NASA CONTRACTOR REPORT

NASA CR

NASA CR-2776

ANALYSIS OF PLASMAS GENERATED BY FISSION FRAGMENTS

Jerry E. Deese and H. A. Hassan

Prepared by
NORTH CAROLINA STATE UNIVERSITY
Raleigh, N.C. 27607
for Langley Research Center

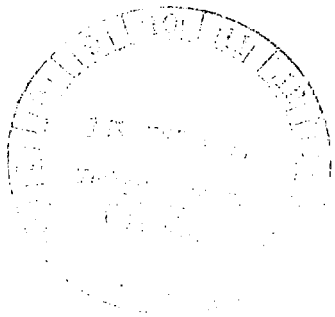

NATIONAL AERONAUTICS AND SPACE ADMINISTRATION • WASHINGTON, D. C. • JANUARY 1977

1. Report No.	2. Government Accession No.	3. Recipient's Catalog No.
NASA CR-2776		

4. Title and Subtitle	5. Report Date
ANALYSIS OF PLASMAS GENERATED BY FISSION FRAGMENTS	January 1977
	6. Performing Organization Code

7. Author(s)	8. Performing Organization Report No.
Jerry E. Deese and H. A. Hassan	
	10. Work Unit No.

9. Performing Organization Name and Address	11. Contract or Grant No.
North Carolina State University Raleigh, North Carolina 27607	NSG 1058
	13. Type of Report and Period Covered
12. Sponsoring Agency Name and Address	Contractors Report
National Aeronautics and Space Administration Washington, D. C. 20546	14. Sponsoring Agency Code

15. Supplementary Notes

Project Manager, Frank Hohl, Space Systems Division, NASA Langley Research Center, Hampton, Virginia

Topical report.

16. Abstract

A kinetic model is developed for a plasma generated by fission fragments and the results are employed to study He plasma generated in a tube coated with fissionable material. Because both the heavy particles and electrons play important roles in creating the plasma, their effects are considered simultaneously. The calculations are carried out for a range of neutron fluxes and pressures. In general, the predictions of the theory are in good agreement with available intensity measurements. Moreover, the theory predicts the experimentally measured inversions. However, the calculated gain coefficients are such that lasing is not expected to take place in a helium plasma generated by fission fragments. The effects of an externally applied electric field are also considered.

17. Key Words (Suggested by Author(s))	18. Distribution Statement
Fission Produced Plasmas Nuclear Pumped Lasers	Unclassified - Unlimited Subject Category 75

19. Security Classif. (of this report)	20. Security Classif. (of this page)	21. No. of Pages	22. Price*
Unclassified	Unclassified	50	$3.75

* For sale by the National Technical Information Service, Springfield, Virginia 22161

ANALYSIS OF PLASMAS GENERATED BY FISSION FRAGMENTS

Jerry E. Deese and H. A. Hassan

North Carolina State University

SUMMARY

A kinetic model is developed for a plasma generated by fission fragments and the results are employed to study He plasma generated in a tube coated with fissionable material. Because both the heavy particles and electrons play important roles in creating the plasma, their effects are considered simultaneously. The calculations are carried out for a range of neutron fluxes and pressures. In general, the predictions of the theory are in good agreement with available intensity measurements. Moreover, the theory predicts the experimentally measured inversions. However, the calculated gain coefficients are such that lasing is not expected to take place in a helium plasma generated by fission fragments. The effects of an externally applied electric field are also considered.

INTRODUCTION

Increased interest in gas core reactors[1] and the recent demonstration of direct nuclear pumping[2-5] focused attention on plasmas generated by the high energy fission fragments. Such systems are rather complex and the plasma generated in them is, in general, not in thermal equilibrium. Therefore, before one can predict their performance characteristics, one needs to develop a detailed and self-consistent kinetic model capable of predicting the behavior of the plasmas generated in these devices.

Several authors have analyzed the space-dependent volumetric production of ions by fission fragments passing through a background gas. Both Leffert, et al.[6] and Nguyen and Grossman[7] derived expressions for the spatial distribution of fission fragment ion production. In both of these analyses an energy independent empirical value W is assumed for the amount of energy required to produce an ion pair. The former utilized both linear and square energy-loss models for the heavy particles, while Nguyen and Grossman used the Bohr stopping equation for fission fragments. Rather than rely on an empirical constant Miley and Thiess[8,9] derived an expression for the ionization and excitation rates which takes into account the effect of the energy distribution of the incident particles. Such a calculation requires estimation of the energy dependent cross sections for excitation and ionization by heavy charged particles. A Bethe-Born type representation was employed for the case of helium excitation by alpha particles and fission fragments[8,9], and later Guyot, et al.[10] employed Gryzinski cross sections[11] for helium ionization by alpha particles and lithium ions.

The calculation of the electron energy distribution function in electric discharges and in the absence of a high energy volumetric source is a standard procedure. However, there are only a few analyses of distributions resulting from a flux of high energy particles where there is a high energy volumetric electron source. Calculations using a Monte Carlo method were carried out by Wang and Miley[12]. Later, Lo and Miley[13] used a simplified version of the Boltzmann equation to determine the electron energy distribution in a helium plasma produced by a mono-energetic electron source. More recently, Hassan and Deese[14] presented a more elaborate Boltzmann equation formulation which took into consideration the primary electron spectrum.

In general, theoretical studies of excited state densities have assumed the electron distribution function to be a Maxwellian at some characteristic temperature. Russell[15] used such an assumption in calculating excited state densities in argon. Leffert, et al.[6] and Rees, et al.[16] also studied noble gas plasmas assuming the electron distribution function to be Maxwellian. More recently Maceda and Miley[17] calculated the number densities of the helium excited states using the non-Maxwellian distributions of Lo and Miley[13]; their results indicate a number of possible inversions.

In addition to the above analyses, there exists a number of experimental investigations dealing with nuclear pumped lasers and laser enhancement. Work carried out before 1972 is summarized in reference 18 while a summary of the nuclear laser effort at the University of Illinois along with an exhaustive list of references on virtually every aspect of radiation produced noble gas plasmas is included in the work of Thiess[19]. Of particular interest here are experiments studying individual atomic transitions at various pressures and additive concentrations under fission fragment excitation. The earliest study of fission fragment excited spectra is that of Morse, et al.[20] who examined the effects of fission fragment radiation on He, Ar, N_2, and air. Guyot[21] measured the production of helium metastables by $B^{10}(n,\alpha)$ fission fragments, while Walters[22] measured the relative intensities of the various transitions in both helium and argon.

As a result of the numerous research efforts outlined above, actual nuclear pumped lasing has just recently been reported by several authors. McArthur and Tollefsrud[2] reported lasing action in carbon monoxide as a result of nuclear excitation only. Helmick, et al.[3] demonstrated direct nuclear pumping in He-Xe gas mixtures. A third case of direct nuclear pumped lasing is that of DeYoung[4]

in a neon-nitrogen mixture. All of the above lasers employed tubes coated with fissionable material. The work of Jalufka, et al.[5] employed a volume source of fission fragments; the $^{3}He(n,P)^{3}H$ reaction was employed to excite a ^{3}He-Ar laser. Obviously the nuclear pumped gas laser research effort is still in its early stages with the validity of the concept having been demonstrated only recently.

The object of this investigation is the development of a theoretical model for a plasma generated by high energy fission fragments. The kinetic model treats particles in different quantum states as different species and uses the multifluid conservation equations of mass, momentum and energy to describe the resulting system. It takes into consideration the following kinetic processes: ionization, excitation and deexcitation, radiative recombination, spontaneous emission, associative ionization and dissociative and collisional recombination. Because both the heavy particles and electrons play important roles in creating the plasma, their effects are considered simultaneously. The rates of reactions involving electrons were calculated using electron distribution functions obtained from a solution of a Boltzmann equation appropriate for plasmas generated by fission fragments[14].

The above model is employed to study a helium plasma generated by fission fragments. Helium was chosen because of the availability of experimentally measured cross sections and rates and in-reactor measurements[22]. In general, the results show good agreement with experiment. Moreover, they indicate a number of possible laser transitions; all of them, however, are in the IR region.

ANALYTICAL FORMULATION

The systems to be modeled here are those appropriate for nuclear pumped lasers. Typically, they consist of tubes coated with fissionable material and filled with gas at some given pressure and temperature. The tube is placed in the high neutron flux region of a reactor. Under neutron bombardment fission fragments emerge from the coating and enter the gas. The ensuing energy transfer results in ionization and excitation of the background gas. A schematic of the slab geometry employed in this analysis is shown in figure 1.

Treating particles in different excited states as different species one can utilize the multifluid conservation equations to describe the plasma generated by the fission fragments. For the conditions under consideration, the steady state approximation is appropriate. In this approximation, the effects of gradients are assumed negligible. Thus, the conservation of species equations,

$$\frac{\partial n_s}{\partial t} + \nabla \cdot (n_s \vec{U}_s) = I_s + R_s \tag{1}$$

reduces, as a result of this approximation, to

$$I_s + R_s = 0 \quad . \tag{2}$$

In the above equations, s is a charged particle or any quantum state of the background gas and, for species s, n_s is the number density, $\vec{U}_s$ is the velocity and I_s and R_s are the production rates per unit volume resulting from nuclear and kinetic sources, respectively.

For very low Mach numbers the momentum equation reduces to

$$p \simeq \text{const.} \tag{3}$$

where p is the pressure, while the energy equation takes the form

$$P_i = Q \tag{4}$$

where P_i is the power input and Q is the conduction and radiation losses. For an optically thin highly conducting gas, equation (4) reduces to

$$T \simeq T_i \tag{5}$$

where T_i is the initial gas temperature.

The properties of the electrons are determined from an electron Boltzmann equation. The equation employed is that developed in reference 14. For the high pressures of interest the plasmas generated by the fission fragments are slightly ionized. Therefore, using the Lorentz gas approximation, the resulting Boltzmann equation for a quasi-steady plasma can be written as[14]

$$-\frac{v}{3}\frac{\partial}{\partial x_i}\left(-\frac{v}{\nu_o}\frac{\partial f_o}{\partial x_i}+\frac{eE_i}{m\nu_o}\frac{\partial f_o}{\partial v}\right)+\frac{eE_i}{3mv^2}\frac{\partial}{\partial v}\left[v^2\left(-\frac{v}{\nu_o}\frac{\partial f_o}{\partial x_i}+\right.\right.$$

$$\left.\left.\frac{eE_i}{m\nu_o}\frac{\partial f_o}{\partial v}\right)\right]+\frac{m}{M}\frac{1}{v^2}\frac{\partial}{\partial v}\left[\nu_o v^2\left(vf_o+\frac{kT}{m}\frac{\partial f_o}{\partial v}\right)\right]+$$

$$\frac{N}{v}\sum\left[v'^2\,Q_s(v')f_o'-v^2\,Q_s(v)f_o\right]+\left(\partial f_o/\partial t\right)_c=0\ , \tag{6}$$

where

$$\frac{1}{2}mv'^2=\frac{1}{2}mv^2+\frac{1}{2}mv_s^2\ , \tag{7}$$

v is the velocity, e is the electric charge, m is the electronic mass, M is the mass of the heavy particles, N is the gas number density, ν_o is the collision frequency, $1/2\ mv_s^2$ is the excitation energy, Q_s is the excitation cross section and $(\partial f_o/\partial t)_c$ is the source term resulting from primary and secondary ionization and recombination. An explicit expression for $(\partial f_o/\partial t)_c$ together with the method of solution of equation (6) is given in reference 14.

The quantities I_s and R_s must be determined before the above system of equations can be solved for the various species present. To determine I_s and

R_s, one needs to specify the important kinetic processes in the system. The major reactions included here, which are appropriate for noble gases, are

1. Fission fragment excitation

$$ff + X \rightarrow X_j + ff$$

2. Fission fragment ionization

$$ff + X \rightarrow X^+ + e + ff$$

3. Spontaneous emission

$$X_i \rightarrow X_j + h\nu$$

4. Ionization and recombination

$$X_i + e \rightleftarrows X^+ + e + e$$

5. Electron excitation and de-excitation

$$X_i + e \rightleftarrows X_j + e$$

6. Radiative recombination

$$X^+ + e \rightarrow X + h\nu$$

7. Excitation transfer

$$X_j + X \rightleftarrows X_k + X$$

8. Dissociative recombination

$$X_2^+ + e \rightarrow X_i + X$$

9. Collisional recombination

$$X^+ + X + X \rightarrow X_2^+ + X$$

10. Associative ionization

$$X + X_i \rightarrow X_2^+ + e$$

11. Electron stabilized recombination

$$X_2^+ + e + e \rightarrow X_i + X + e$$

12. Neutral stabilized recombination

$$X_2^+ + e + X \rightarrow X_i + X + X$$

13. Metastable ionization

$$X^* + X^* \rightarrow X^+ + X + e$$

14. Charge transfer

$$X^+ + M \rightarrow M^+ + X$$

15. Penning ionization

$$X^* + M \rightarrow M^+ + X + e \tag{8}$$

where M represents a substance other than the background gas, or an impurity.

The term I_s is a result of reactions of Type 1 and 2 while R_s is obtained from reactions of Type 3-15. In general, for a reaction of the type

$$a_i A_i + a_j A_j \rightarrow a_s A_s + a_t A_t \tag{9}$$

the contribution to the production rate of species s is

$$a_s K n_k^{a_i} n_j^{a_j} \tag{10}$$

where $a_\ell (\ell = i, j, s, t)$ denotes a stochiometric coefficient. The quantity K is the forward rate coefficient and is given by

$$K = \int f_i f_j g_{ij} \sigma_{ij} d\vec{V}_i d\vec{V}_j \tag{11}$$

where, for species i, f_i is the energy distribution function, $\vec{V}_i$ is the velocity, $g_{ij} = |\vec{V}_i - \vec{V}_j|$ and σ_{ij} is the collision cross section. If i represents the stationary background gas and j a fission fragment or an electron, then equation (11) reduces to

$$K = \int f_j \sigma V_j \, d\vec{V}_j \quad . \tag{12}$$

The rate coefficients for reactions involving the background gas (or gases) are usually obtained from experiment. On the other hand reactions involving the fission fragments and electrons can, in principle, be calculated according to equation (12) from collision cross sections determined from experiment or theory and appropriate distribution functions. In this work the electron distribution function is calculated from equation (6). Unfortunately, the situation with regards to fission fragments is not well understood; this is because the fission fragments are characterized by initial energies ranging from 50 to 115 Mev, initial charges from 16e to 24e and masses from 70 to 160 atomic mass units. In addition no data is available on cross sections for ionization and excitation by fission fragments. Because of these uncertainties, the contribution of the fission fragments to excitation and ionization was estimated using two different approximate methods. In the first, the procedure outlined in reference 6 was used to estimate the average energy deposited in the gas per unit volume per unit time, E_f. The average number of ions produced per unit volume per unit time is given by dividing E_f by W, the energy expended per ion pair produced. Similarly, the total number of excited states produced is determined by dividing E_f by W_{ex}, the energy expended per excited state produced. Rees, et al.[16] determined that the total excited particle production rate from fission fragments is .53 times the ion production rate, thus

$$W_{ex} = W/.53 \quad . \tag{13}$$

This procedure determines only the total number of excited states produced by fission fragments and some model for the distribution of these states must be adopted. Because of the absence of a generally accepted procedure for the

distribution of excited states a number of models have been employed here and these are discussed under Results and Discussions.

The other approach uses the procedure of Thiess and Miley[9], or Guyot, et al.[10], which is based on a heavy particle distribution function derived from a semiempirical slowing law together with ionization and excitation cross sections based on the Born or the Gryzinski approximations. To utilize this procedure one needs to assume that the fission fragments fall into two groups: a light group with an average mass number of 96, an average charge of 20e and an average initial energy of 98 Mev; and a heavy group with an average mass number of 140, an average charge of 22e and an average initial energy of 67 Mev. A convenient summary of all formulas needed to calculate the contribution of the fission fragments to ionization and excitation by the two methods outlined above is given in reference 10.

RESULTS AND DISCUSSION

The above model is applied to a study of He plasma generated by fission fragments and the results are compared with the measurements of Walters[22] who employed a tube of radius 1.85 cm coated with U_3O_8. To conform to the conditions of the experiment, the calculations allow for the presence of a nitrogen impurity in the system. For a given pressure, temperature, neutron flux and tube dimensions, the above model is capable of predicting the number densities of the helium excited states, the atomic and molecular ions and the electrons. From this, one can calculate the relative intensities and gain coefficients. For the calculations presented here, the gas temperature is assumed constant at 300°K, while the pressure ranges from 100-760 Torr (1 Torr = 133 N/m^2), the

neutron flux from $3.8 \times 10^{11} - 10^{16}$ neutrons/cm^{2}sec. and the nitrogen concentration from .001 to 50 parts per million.

All helium excited states with a principal quantum number of 5 or less are included in the calculations. The rates or cross sections for the reactions of Types 3 through 15 indicated in equation (8) were obtained from references 23-54 while Einstein coefficients for spontaneous emission were taken from references 55 and 56. A listing of the reactions included in the analysis with references to cross section and rate data is given in Appendix A. Because the experimental data is incomplete the products or the rates of some reactions had to be estimated and these are discussed next.

At the high pressures of interest here the recombination process in noble gases is complicated by the formation of molecular ions. For pressures greater than 5 Torr the reaction

$$\mathrm{He}^+ + 2\ \mathrm{He} \rightarrow \mathrm{He}_2^+ + \mathrm{He} \tag{14}$$

quickly converts atomic ions into molecular ions[23]. The molecular ion recombination is governed by three reactions[24,25]

$$\begin{aligned} e + \mathrm{He}_2^+ &\rightarrow \mathrm{He} + \mathrm{He}^* \\ e + e + \mathrm{He}_2^+ &\rightarrow \mathrm{He} + \mathrm{He}^* + e \\ e + \mathrm{He} + \mathrm{He}_2^+ &\rightarrow 2\ \mathrm{He} + \mathrm{He}^* \end{aligned} \tag{15}$$

where He^* denotes an excited state. The distribution of excited states produced by these reactions is not well known. However, recent studies[25-27] indicate that at least 70% of the excited states produced are atomic metastables in the pressure range of interest here. Although potential energy curves indicate other states such as the 2^3P states are produced in molecular ion

recombination[57], it is assumed that He^* in the reactions indicated in equation (15) are atomic metastables.

Rates for associative ionization are available for atomic states of principal quantum number 3 and triplet states of principal quantum number 4, references 26, 28-30. Cross sections for the excitation transfer reactions are available for n = 2 and n = 3 but only for the triplet states when n = 4, reference 26. Because these processes are important in the determination of the final distribution of excited states some estimate of the unavailable rates is required. It is assumed here that the associative ionization rates for n = 5 states are the same as the corresponding n = 4 states while the associative ionization cross sections for the n^1F states are assumed equal to those for the n^1D states. Moreover, three calculations were carried out in which the cross sections for associative ionization and excitation transfer reactions of the triplet n = 4 states were assumed to be one-third of, equal to, and three times the corresponding singlet reaction cross sections. Comparison of calculated and measured excited states showed that better agreement with experiment is obtained when $Q(4^1X) \leq Q(4^3X)$. Therefore, unless indicated otherwise, all calculations reported here employ this assumption.

As indicated earlier, when a 'W' value is used to estimate the total number of excited states further assumptions are needed to indicate which states are excited. From a study of the spectra of noble gases generated by the impact of alpha particles, Bennett[58] suggested that most of the excited states in He are n^1P states with the majority of them in the 2^1P state. His conclusion was based on the fact that calculated excitation cross sections, based on the Born approximation, are highest for the n^1P states. This assumption is contrasted with that of Guyot[21] where he assumed that most of the excited atoms

resulting from the impact of alpha particles are in the 2^1S state and these are converted to the 2^3S states by electron impact. Calculations using both of the above models were carried out; for these calculations a value of W_{ex} = 85 ev was employed.

Comparison of the results with the experiments of Walters[22] requires that the effect of a nitrogen contaminant be taken into consideration. The gas used in the experiment contained a nitrogen contaminant of approximately 50 parts per million. The effect of the pressure on the number densities of the electrons and the two metastable states is given in figure 2 while figure 3 shows the effect of pressure on several of the higher states with and without a 50 parts per million nitrogen contaminant. For these figures, the neutron flux is 3.8×10^{11} neutrons/cm.^{2}sec. Considering pure helium first, it is seen that the electron number density decreases as the pressure increases. This is because the dominant helium recombination process is the neutral stabilized recombination of the molecular ion and this process becomes more efficient as the pressure increases. The dominant processes governing the excited states number densities are electron excitation from the ground state and the metastable state 2^3S, excitation transfer, associative ionization and spontaneous emission. As the pressure increases, the decrease in the electron density coupled with the increased effectiveness of the associative ionization and excitation transfer results in the decrease of the excited states shown in figure 3. Only the 2^3S and 2^1P states show an increase as the pressure increases; the rapid recombination resulting from the last reaction in equation (15) accounts for the 2^3S behavior.

As is seen from figures 2 and 3, the effect of nitrogen on the various species is quite significant. Both the helium molecular ion and the metastables

are quickly converted to nitrogen ions whose dominant recombination process is dissociative recombination. This not only lowers the concentrations of the He ions and metastables but changes the electron number density variation with pressure as well. When nitrogen is present the dominant recombination process is the two-body dissociative recombination. This process does not become more efficient as pressure increases and as a result the electron number density increases with an increase in pressure. Thus, the net effect of nitrogen is two-fold: it lowers the number density of electrons and metastables making electron excitation from metastable states less important and, it changes the number density dependence on pressure. As a result of this, one would expect a significant effect on the higher excited states as well. Because the electron number density increases with pressure the electron excitation rates increase with pressure. Thus, as is seen in figure 3, the marked decrease in excited state population with pressure in the case of pure helium is not as pronounced when nitrogen is present. The figure also shows that the magnitudes of the number densities decrease with pressure.

The results indicated in figure 3 do not exhibit the peak around 200 Torr shown in figure 4-9 of reference 17. Both Walters[22] and Thiess[19] suggest that the associative ionization process may be a three-body process of the form

$$He^{*} + 2\ He \rightarrow He_2^{+} + He \tag{16}$$

rather than the two-body process

$$He^{*} + He \rightarrow He_2^{+} + e \tag{17}$$

assumed here. If this process is indeed three-body in nature its effectiveness will increase with pressure.

A study of the variation of the number densities with neutron flux for the case of a pure helium gas at 100 Torr has also been carried out. The behavior of the electrons and metastables is given in figure 4 and that of some higher states is shown in figure 5. The number densities of the higher states increase linearly with the flux at lower neutron flux levels. As the electron number density increases, the electron stabilized three-body recombination becomes important. Thus, population densities highly dependent on electron excitation rates do not increase as rapidly at higher flux levels.

Because the nitrogen contaminant has a significant effect on the number densities, a determination of the concentration range where its effect becomes insignificant is of interest. Figure 6 shows a plot of the electron and metastable number densities vs. nitrogen concentration at 100 Torr and a neutron flux of 3.8×10^{11} neutrons/cm^{2}sec. As is seen from the figure, the effect of nitrogen is negligible below a concentration of 10^{-8}.

All of the above results assume the 2^1P state to be the only excited state produced by fission fragments. Calculations using the procedure of reference 9, the TM model, have also been carried out. Boltzmann plots showing $\log \lambda I/g_i A = \log[hcn_i/4\pi g_i]$, where λ is the wave length, I is the intensity, A is Einstein's transition probability, g_i is the degeneracy, h is Planck's constant and c is the speed of light, vs. ε_u, the energy of the upper level, for pressures of 100 and 760 Torr are given in figures 7 and 8 for the 2^1P model and in figures 9 and 10 for the TM model. Error bars in these graphs indicate the spread in Walters' experimental data. Using the TM model, the triplet states are considerably underpopulated relative to the singlet states. Because Walters found the triplet states to be of the same order of magnitude for states with n = 3, it appears that the 2^1P model is more appropriate.

As is seen from figure 7, the 2^1P model gives good agreement with experiment at 100 Torr; the only discrepancy being the n^3D states which are overpopulated compared with the experimental measurements. At 760 Torr the agreement of the 2^1P model with experiment is not as good as at 100 Torr. All triplet states except the 3^3S are predicted to have a population greater than experimentally measured values. This could be due to an improper pressure dependence for associative ionization as discussed earlier. In general, singlet states have much higher emission coefficients and as a result, cascade losses play a larger role in the singlet system. The triplet system on the other hand is predominantly governed by associative ionization and excitation transfer processes and these have a greater dependence on pressure. Thus, it is expected that triplet states number densities will decrease more rapidly with pressure. Calculations have also been carried out assuming fission fragments produce only 2^1S states. However, for this case the 2^1S number density is higher than the 2^3S number density and this is not in agreement with available experiments[21].

When studying pure helium, two population inversions have been found throughout the entire range of pressures, neutron fluxes and fission fragment excitation models examined on the $3^1P - 3^1D$ (95.76μ) and $4^1P - 4^1D$ (216μ) lines[22,59]. In addition, for pressures less than 200 Torr and neutron fluxes less than 10^{14} neutrons/cm.^{2}sec. the TM model predicts an inversion of the $3^1S - 2^1P$ line (7281 Å). The expression for the gain coefficient is given in Appendix B. The gain coefficients together with other inversions, operating conditions and fission fragment models employed are summarized in Table 1. The addition of the nitrogen did not change the above results. However, the gain coefficients are slightly decreased because of greater depopulation of excited levels.

TABLE 1 GAIN COEFFICIENTS

Transition	Wavelength	Excitation Model	Pressure Torr	Neutron Flux	n_{N_2}/n_T	Gain Coefficient
$3^1P - 3^1D$	95.76 μ	2^1P	100	3.8×10^{11}	0.0	0.28×10^{-9}
$3^1P - 3^1D$	95.76 μ	2^1P	760	3.8×10^{11}	0.0	0.76×10^{-11}
$3^1P - 3^1D$	95.76 μ	2^1P	100	1.0×10^{16}	0.0	0.14×10^{-5}
$3^1P - 3^1D$	95.76 μ	2^1P	760	3.8×10^{11}	5×10^{-5}	0.42×10^{-11}
$3^1P - 3^1D$	95.76 μ	TM	760	3.8×10^{11}	0.0	0.15×10^{-9}
$4^1P - 4^1D$	216 μ	2^1P	100	3.8×10^{11}	0.0	0.12×10^{-9}
$4^1P - 4^1D$	216 μ	2^1P	760	3.8×10^{11}	0.0	0.24×10^{-11}
$4^1P - 4^1D$	216 μ	2^1P	100	1.0×10^{16}	0.0	0.16×10^{-6}
$4^1P - 4^1D$	216 μ	2^1P	760	3.8×10^{11}	5×10^{-5}	0.14×10^{-11}
$4^1P - 4^1D$	216 μ	TM	760	3.8×10^{11}	0.0	0.11×10^{-10}
$4^3D - 4^3P$	43.94 μ	2^1P	100	1.0×10^{16}	0.0	0.20×10^{-5}
$3^1S - 2^1P$	7281 Å	TM	100	3.8×10^{11}	0.0	0.24×10^{-8}

Figures 7-10 show only states of principal quantum number four or less; these states were the only states considered in the determination of the inversions present. Excitation transfer cross sections are not available for the n = 5 states and as a result these states are overpopulated. The importance of these reactions can be seen by performing calculations where these reactions are neglected for all states. The Boltzmann plot for such a case is shown in figure 11. Comparing figures 7 and 11, it is clear that excitation transfer plays an important role in determining the relative population of excited states and consequently, the presence of inversion. Similar conclusions hold when one assumes

$$Q(4^1X) = 3\ Q(4^3X)\ , \tag{18}$$

as is seen from comparing figures 7 and 12.

Calculations have also been carried out in the presence of an externally applied electric field of 10 V/cm and the results are shown in figure 13. For this calculation the pressure is 100 Torr, the neutron flux is 3.8×10^{11} neutrons/cm^2.sec. and the background gas is pure helium. As is seen from the figure the $n^1P - n^1D$ inversions present in the absence of an electric field disappear and a new inversion $4^3D - 4^3P$ (43.94μ) appears. The gain coefficient for this transition is 7.5×10^{-2} which reflects the large increase in the transfer of electron energy to the excited states[14]. It should be noted that this result is for the particular conditions specified above and no attempt has been made to study systematically the effect of an externally applied electric field on a nuclear pumped laser.

Recently, Jalufka, et al.[5] demonstrated a volumetric nuclear-pumped laser using $^3He(n,P)^3H$ reaction to excite a ^3He - Ar laser. The method presented

here can, with slight modification be used to analyze this new mode of nuclear pumping.

CONCLUDING REMARKS

Considering the incompleteness of available cross sections, the predictions of the model are in good agreement with available relative intensity measurements and measured inversions. However, more complete rate data are needed for the accurate predictions of other possible inversions involving the higher states. The calculated gain coefficients are so small that, because of cavity losses, lasing is not expected to occur in helium. Thus, helium is not a good candidate for a nuclear pumped laser. The results also suggest the desirability of studying the effects of an externally applied electric field on nuclear pumped lasers.

APPENDIX A

REACTIONS INCLUDED IN THE ANALYSIS

A listing of the reactions included in the analysis with references to cross sections and rate data is given below. If a reference is not indicated then the reaction is treated in the manner outlined under Results and Discussion. The principles of microscopic reversibility and detailed balancing are used, where appropriate, to relate forward and backward cross sections and rates, respectively.

	REACTION	REFERENCES
	Type 3: $X_i \rightarrow X_j + h\nu$	55,56
	Type 4: $X_i + e \rightleftarrows X^+ + e + e$	
(1)	$He + e \rightleftarrows He^+ + e + e$	31
	Type 5: $X_i + e \rightleftarrows X_j + e$	
(2)	$He + e \rightleftarrows He(2^1S) + e$	32,33,34,35
(3)	$He + e \rightleftarrows He(3^1S) + e$	36
(4)	$He + e \rightleftarrows He(4^1S) + e$	36,37
(5)	$He + e \rightleftarrows He(5^1S) + e$	36,37
(6)	$He + e \rightleftarrows He(2^1P) + e$	38
(7)	$He + e \rightleftarrows He(3^1P) + e$	36,37
(8)	$He + e \rightleftarrows He(4^1P) + e$	36,37
(9)	$He + e \rightleftarrows He(5^1P) + e$	37,39
(10)	$He + e \rightleftarrows He(3^1D) + e$	36,37

(11)	$He + e \rightleftarrows He(4^1D) + e$	36,37
(12)	$He + e \rightleftarrows He(5^1D) + e$	36,37
(13)	$He + e \rightleftarrows He(4^1F) + e$	40
(14)	$He + e \rightleftarrows He(5^1F) + e$	40
(15)	$He + e \rightleftarrows He(2^3S) + e$	32,33,34
(16)	$He + e \rightleftarrows He(3^3S) + e$	36
(17)	$He + e \rightleftarrows He(4^3S) + e$	36,37
(18)	$He + e \rightleftarrows He(5^3S) + e$	36
(19)	$He + e \rightleftarrows He(2^3P) + e$	38
(20)	$He + e \rightleftarrows He(3^3P) + e$	36,37
(21)	$He + e \rightleftarrows He(4^3P) + e$	36
(22)	$He + e \rightleftarrows He(5^3P) + e$	39
(23)	$He + e \rightleftarrows He(3^3D) + e$	36,37
(24)	$He + e \rightleftarrows He(4^3D) + e$	36,37
(25)	$He + e \rightleftarrows He(5^3D) + e$	36
(26)	$He + e \rightleftarrows He(4^3F) + e$	40
(27)	$He + e \rightleftarrows He(5^3F) + e$	40
(28)	$He(2^3S) + e \rightleftarrows He(2^1S) + e$	41
(29)	$He(2^3S) + e \rightleftarrows He(3^1S) + e$	40
(30)	$He(2^3S) + e \rightleftarrows He(4^1S) + e$	40
(31)	$He(2^3S) + e \rightleftarrows He(5^1S) + e$	40

(32) $He(2^3S) + e \rightleftarrows He(2^1P) + e$ 40

(33) $He(2^3S) + e \rightleftarrows He(3^1P) + e$ 40

(34) $He(2^3S) + e \rightleftarrows He(4^1P) + e$ 40

(35) $He(2^3S) + e \rightleftarrows He(5^1P) + e$ 40

(36) $He(2^3S) + e \rightleftarrows He(3^1D) + e$ 40

(37) $He(2^3S) + e \rightleftarrows He(4^1D) + e$ 40

(38) $He(2^3S) + e \rightleftarrows He(5^1D) + e$ 40

(39) $He(2^3S) + e \rightleftarrows He(4^1F) + e$ 40

(40) $He(2^3S) + e \rightleftarrows He(5^1F) + e$ 40

(41) $He(2^3S) + e \rightleftarrows He(3^3S) + e$ 40

(42) $He(2^3S) + e \rightleftarrows He(4^3S) + e$ 40

(43) $He(2^3S) + e \rightleftarrows He(5^3S) + e$ 40

(44) $He(2^3S) + e \rightleftarrows He(2^3P) + e$ 42

(45) $He(2^3S) + e \rightleftarrows He(3^3P) + e$ 40

(46) $He(2^3S) + e \rightleftarrows He(4^3P) + e$ 40

(47) $He(2^3S) + e \rightleftarrows He(5^3P) + e$ 40

(48) $He(2^3S) + e \rightleftarrows He(3^3D) + e$ 40

(49) $He(2^3S) + e \rightleftarrows He(4^3D) + e$ 40

(50) $He(2^3S) + e \rightleftarrows He(5^3D) + e$ 40

(51) $He(2^3S) + e \rightleftarrows He(4^3F) + e$ 40

(52) $He(2^3S) + e \rightleftarrows He(5^3F) + e$ 40

(53) $He(2^3P) + e \rightleftarrows He(2^1P) + e$ 42

(54) $He(2^1S) + e \rightleftarrows He(2^1P) + e$ 42

(55) $He(3^1S) + e \rightleftarrows He(3^1P) + e$ 30,43

(56) $He(3^1S) + e \rightleftarrows He(3^1D) + e$ 30,43

(57) $He(3^3S) + e \rightleftarrows He(3^3P) + e$ 30,43

(58) $He(3^3S) + e \rightleftarrows He(3^3D) + e$ 30,43

(59) $He(3^1P) + e \rightleftarrows He(3^1D) + e$ 30,43

(60) $He(3^3P) + e \rightleftarrows He(3^3D) + e$ 30,43

Type 6: $X^+ + e \rightarrow X + h\nu$

(61) $He^+ + e \rightarrow He + 24.586$ ev 44,45

Type 7: $X_j + X \rightleftarrows X_k + X$

(62) $He(3^1P) + He \rightleftarrows He(3^1S) + He$ 30,43

(63) $He(3^3P) + He \rightleftarrows He(3^3S) + He$ 26,30,43

(64) $He(3^1P) + He \rightleftarrows He(3^1D) + He$ 30,43

(65) $He(3^3P) + He \rightleftarrows He(3^3D) + He$ 26,30,43

(66) $He(3^3S) + He \rightleftarrows He(2^3P) + He$ 26

(67) $He(3^1S) + He \rightleftarrows He(2^1P) + He$ 26

(68) $He(4^3S) + He \rightleftarrows He(3^3S) + He$ 26

(69) $He(4^3S) + He \rightleftarrows He(3^3P) + He$ 26

(70) $He(4^3S) + He \rightleftarrows He(3^3D) + He$ 26

(71) $He(4^3P) + He \rightleftarrows He(3^3S) + He$ 26

(72) $He(4^3P) + He \rightleftarrows He(3^3P) + He$ 26

(73) $He(4^3P) + He \rightleftarrows He(3^3D) + He$ 26

(74) $He(4^3D) + He \rightleftarrows He(3^3S) + He$ 26

(75) $He(4^3D) + He \rightleftarrows He(3^3P) + He$ 26

(76) $He(4^3D) + He \rightleftarrows He(3^3D) + He$ 26

(77) $He(4^3F) + He \rightleftarrows He(3^3S) + He$

(78) $He(4^3F) + He \rightleftarrows He(3^3P) + He$

(79) $He(4^3F) + He \rightleftarrows He(3^3D) + He$

(80) $He(4^1P) + He \rightleftarrows He(4^{1,3}F) + He$ 46,47

(81) $He(5^1P) + He \rightleftarrows He(5^{1,3}F) + He$ 46,47

(82) $He(2^1S) + He \rightleftarrows He(1^1S) + He$ 48

(83) $He(4^1S) + He \rightleftarrows He(3^1S) + He$

(84) $He(4^1S) + He \rightleftarrows He(3^1P) + He$

(85) $He(4^1S) + He \rightleftarrows He(3^1D) + He$

(86) $He(4^1P) + He \rightleftarrows He(3^1S) + He$

(87) $He(4^1P) + He \rightleftarrows He(3^1P) + He$

(88) $He(4^1P) + He \rightleftarrows He(3^1D) + He$

(89) $He(4^1D) + He \rightleftarrows He(3^1S) + He$

(90) $He(4^1D) + He \rightleftarrows He(3^1P) + He$

(91) $He(4^1D) + He \rightleftarrows He(3^1D) + He$

(92) $He(4^1F) + He \rightleftarrows He(3^1S) + He$

(93) $He(4^1F) + He \rightleftarrows He(3^1P) + He$

(94) $He(4^1F) + He \rightleftarrows He(3^1D) + He$

Type 8: $X_2^+ + e \rightleftarrows X_i + X$

(95) $He_2^+ + e \rightarrow He(2^3S) + He$ 25,26,27

(96) $He_2^+ + e \rightarrow He(2^1S) + He$ 25,26,27

Type 9: $X^+ + X + X \rightarrow X_2^+ + X$

(97) $He^+ + 2\ He \rightarrow He_2^+ + He$ 23

Type 10: $X_i + X \rightarrow X_2^+ + e$

(98) $He(3^1S) + He \rightarrow He_2^+ + e$ 28,29,30

(99) $He(3^1P) + He \rightarrow He_2^+ + e$ 28,29,30

(100) $He(3^1D) + He \rightarrow He_2^+ + e$ 28,29,30

(101) $He(3^3S) + He \rightarrow He_2^+ + e$ 26,28,29,30

(102) $He(3^3P) + He \rightarrow He_2^+ + e$ 26,28,29,30

(103) $He(3^3D) + He \rightarrow He_2^+ + e$ 26,28,29,30

(104) $He(4^1S) + He \rightarrow He_2^+ + e$

(105) $He(4^1P) + He \rightarrow He_2^+ + e$

(106) $He(4^1D) + He \rightarrow He_2^+ + e$

(107) $He(4^1F) + He \rightarrow He_2^+ + e$

(108) $He(4^3S) + He \rightarrow He_2^+ + e$ 26

(109) $He(4^3P) + He \rightarrow He_2^+ + e$ 26

(110) $He(4^3D) + He \rightarrow He_2^+ + e$ 26

(111) $He(4^3F) + He \rightarrow He_2^+ + e$

(112) $He(5^1S) + He \rightarrow He_2^+ + e$

(113) $He(5^1P) + He \rightarrow He_2^+ + e$

(114) $He(5^1D) + He \rightarrow He_2^+ + e$

(115) $He(5^1F) + He \rightarrow He_2^+ + e$

(116) $He(5^3S) + He \rightarrow He_2^+ + e$

(117) $He(5^3P) + He \rightarrow He_2^+ + e$ 49

(118) $He(5^3D) + He \rightarrow He_2^+ + e$

(119) $He(5^3F) + He \rightarrow He_2^+ + e$

Type 11: $X_2^+ + e + e \rightarrow X_i + X + e$

(120) $He_2^+ + e + e \rightarrow He(2^1S) + He(1^1S) + e$ 24,25

(121) $He_2^+ + e + e \rightarrow He(2^3S) + He(1^1S) + e$ 24,25

Type 12: $X_2^+ + e + e \rightarrow X_i + X + e$

(122) $He_2^+ + e + He \rightarrow He(2^1S) + He + He$ 24,25

(123) $He_2^+ + e + He \rightarrow He(2^3S) + He + He$ 24,25

Type 13: $X^* + X^* \rightarrow X^+ + X + e$

(124) $He(2^1S) + He(2^1S) \rightarrow He^+ + He + e$ 40,41

(125) $He(2^1S) + He(2^3S) \rightarrow He^+ + He + e$ 40,41

(126) $He(2^3S) + He(2^3S) \rightarrow He^+ + He + e$ 27,41,50

When nitrogen is present the following reactions are included:

Type 4: $X + e \rightleftarrows X^+ + e + e$

(127) $N_2 + e \rightleftarrows N_2^+ + e + e$ 39

Type 8: $X_2^+ + e \rightarrow X + X$

(128) $N_2^+ + e \rightleftarrows N + N$ 51

Type 14: $X^+ + N_2 \rightarrow N_2^+ + X$

(129) $He^+ + N_2 \rightleftarrows N_2^+ + He$ 52

(130) $He_2^+ + N_2 \rightleftarrows N_2^+ + He + He$ 53

Type 15: $X^* + N_2 \rightarrow N_2^+ + X + e$

(131) $He(2^1S) + N_2 \rightarrow N_2^+ + He + e$ 54

(132) $He(2^3S) + N_2 \rightarrow N_2^+ + He + e$ 54

APPENDIX B

GAIN COEFFICIENT

The possible lasing transitions in atomic helium involve electronic state transitions. The gain coefficient for transition from upper level m to lower level n is

$$\gamma(\nu) = \frac{c^2 g_m}{8\pi \nu^2} A_{mn} \left[\frac{N_m}{g_m} - \frac{N_n}{g_n}\right] G(\nu) \tag{B1}$$

where $G(\nu)$ is the shape factor, N_m and N_n the number densities of states m and n, g_m and g_n are their degeneracies, A_{mn} is the Einstein coefficient of spontaneous emission from level m to level n, and ν is the frequency of the transition.

The shape factor is affected by two processes, Doppler and pressure broadening. In general, for pressures greater than 30 Torr, pressure broadening is dominant. Thus, Doppler broadening is neglected in this analysis. For pressure broadening the shape factor $G(\nu)$ is given by

$$G(\nu) = \frac{2}{\pi \Sigma_t \nu_{st}} \tag{B2}$$

where

$$\nu_{st} = \frac{2}{3} \left[2k \left(\frac{T_s}{m_s} + \frac{T_t}{m_t}\right)\right]^{1/2} Z_{st} n_t \, . \tag{B3}$$

In equation (B3), s represents the lasing gas and t represents other gases present in the system. When summing on t in equation (B2), t can be equal to s.

The quantities Z_{st} can be calculated from the Lennard-Jones potential parameters of the colliding molecules[60-62]

$$Z_{st} = d_{st}^2 \, \Omega^{(2,2)}(T_{st}^*) \tag{B4}$$

$$d_{st} = \sqrt{d_s\, d_t} \tag{B5}$$

$$T^*_{st} = T/\varepsilon^*_{st} \tag{B6}$$

$$\varepsilon^*_{st} = \frac{2\sqrt{\varepsilon^*_s\, \varepsilon^*_t}\sqrt{I^*_s\, I^*_t}}{(I^*_s + I^*_t)} \quad . \tag{B7}$$

The quantity $\Omega^{(2,2)}(T)$ is obtained from the empirical curve fit[63]

$$\Omega^{(2,2)}(T) = \frac{1.16145}{T^{0.14874}} + 0.52487 \exp[-0.7732\, T] + 2.16178 \exp[-2.43787\, T] - 6.435 \times 10^{-4}\, T^{0.14874} \sin\left(\frac{18.0323}{T^{0.7683}} - 7.27371\right). \tag{B8}$$

The required parameters for helium are[60,64]

$$d_s = 2.576 \times 10^{-8} \text{ cm}$$

$$\varepsilon^*_s = 10.22\ ^\circ\text{K}$$

$$I^*_s = 24.586 \text{ ev} \quad .$$

REFERENCES

1. Schneider, R. T.; and Thom, K.: Fissioning Uranium Plasmas and Nuclear-Pumped Lasers. Nuclear Technology, vol. 27, Sept. 1975, pp. 34-50.

2. McArthur, D. A.; and Tollefsrud, P. B.: Observation of Laser Action in CO Gas Excited Only by Fission Fragments. Applied Physics Letters, vol. 26, Feb. 1975, pp. 187-190.

3. Helmick, H. H.; Fuller, J. L.; and Schneider, R. T.: Direct Nuclear Pumping of a Helium-Xenon Laser. Applied Physics Letters, vol. 26, March 1975, pp. 327-328.

4. DeYoung, R. J.: A Direct Nuclear Pumped Neon-Nitrogen Laser. Ph.D. Dissertation, University of Illinois, 1975.

5. Jalufka, N. W.; DeYoung, R. J.; Hohl, F.; and Williams, M. D.: A Nuclear Pumped ^{3}He-Ar Laser Excited by the $^{3}He(n,P)^{3}H$ Reaction. Applied Physics Letters, vol. 29, Aug. 1976, pp. 188-190.

6. Leffert, C. B.; Rees, D. B.; and Jamerson, F. E.: Noble Gas Plasmas Produced by Fission Fragments. Journal of Applied Physics, vol. 37, Jan. 1966, pp. 133-142.

7. Nguyen, D. H.; and Grossman, L. M.: Ionization by Fission Fragments Escaping from a Source Medium. Nuclear Science and Engineering, vol. 30, Nov. 1967, pp. 233-241.

8. Miley, G. H.; and Thiess, P. E.: A Unified Approach to Two-Region Ionization-Excitation Density Calculations. Nuclear Applications, vol. 6, May 1969, pp. 434-451.

9. Thiess, P. E.; and Miley, G. H.: Calculations of Ionization-Excitation Source Rates in Gaseous Media Irradiated by Fission Fragments and Alpha Particles. NASA SP-236, 1971, pp. 369-396.

10. Guyot, J. C.; Miley, G. H.; and Verdeyen, J. T.: Application of a Two Region Heavy Charged Particle Model to Noble-Gas Plasmas Induced by Nuclear Radiations. Nuclear Science and Engineering, vol. 48, Aug. 1972, pp. 130-141.

11. Gryzinski, M.: Classical Theory of Atomic Collisions. I. Theory of Inelastic Collisions. Physical Review, vol. 138, April 1965, pp. A336-A358.

12. Wang, B. W.; and Miley, G. H.: Monte Carlo Simulation of Radiation-Induced Plasma. Nuclear Science and Engineering, vol. 52, Sept. 1973, pp. 130-141.

13. Lo, R. H.; and Miley, G. H.: Electron Energy Distribution in a Helium Plasma Generated by Nuclear Radiation. IEEE Transactions on Plasma Science, vol. PS-2, Dec. 1974, pp. 198-205.

14. Hassan, H. A.; and Deese, J. E.: The Electron Boltzmann Equation in a Plasma Generated by Fission Products. NASA CR-2712, 1976.

15. Russell, G. R.: Feasibility of a Nuclear Laser Excited by Fission Fragments Produced in a Pulsed Nuclear Reactor. NASA SP-236, 1971, pp. 53-62.

16. Rees, D. B.; Leffert, C. B.; and Rose, D. J.: Electron Density in Mixed Gas Plasmas Generated by Fission Fragments. Journal of Applied Physics, vol. 40, March 1969, pp. 1884-1896.

17. Maceda, E. L.; and Miley, G. H.: Non-Maxwellian Electron Excitation in Helium. Bulletin of the American Physical Society, vol. 20, Feb. 1975, p. 255.

18. Thom, K.; and Schneider, R. T.: Nuclear Pumped Gas Lasers. AIAA Journal, vol. 10, April 1972, pp. 400-406.

19. Thiess, P. E.: Optical Emission and Kinetics of High Pressure Radiation-Produced Noble Gas Plasmas. Ph.D. Dissertation, University of Illinois, 1975.

20. Morse, F.; Harteick, P.; and Dondes, S.: Excited Species of Gases Produced in the Nuclear Reactor. Radiation Research, vol. 29, Nov. 1966, pp. 317-328.

21. Guyot, J. C.: Measurement of Atomic Metastable Densities in Noble Gas Plasmas Created by Nuclear Irradiation. Ph.D. Dissertation, University of Illinois, 1971.

22. Walters, R. A.: Excitation and Ionization of Gases by Fission Fragments. Ph.D. Dissertation, University of Florida, 1973.

23. Beaty, E. C.; and Patterson, P. L.: Mobilities and Reaction Rates of Ions in Helium. Physical Review, vol. 137, Jan. 1965, pp. A346-A357.

24. Berlande, J.; Cheret, M.; Deloche, R.; Gonfalone, A.; and Manus, C.: Pressure and Electron Density Dependence of the Electron-Ion Recombination Coefficient in He. Physical Review A, vol. 1, March 1970, pp. 887-896.

25. Deloche, R.; Monchicourt, P.; Cheret, M.; and Lambert, F.: High-Pressure Helium Afterglow at Room Temperature. Physical Review A, vol. 13, March 1976, pp. 1140-1176.

26. Cohen, J. S.: Multistate Curve-Crossing Model for Scattering: Associative Ionization and Excitation Transfer in Helium. Physical Review A, vol. 13, Jan. 1976, pp. 99 - 114.

27. Johnson, A. W.; and Gerardo, J. B.: Ionizing Collisions of Two Metastable Helium Atoms (2^3S). Physical Review A, vol. 7, March 1973, pp. 925A-928A.

28. Teter, M. P.; Niles, F. E.; and Robertson, W. W.: Hornbeck-Molnar Cross Sections for the n = 3 States of Helium. The Journal of Chemical Physics, vol. 44, April 1966, pp. 3018-3021.

29. Wellenstein, H. F.; and Robertson, W. W.: Collisional Relaxation Processes for the n = 3 States of Helium. II. Associative Ionization. The Journal of Chemical Physics, vol. 56, Feb. 1972, pp. 1077-1082.

30. Wellenstein, H. F.; and Robertson, W. W.: Collisional Relaxation Processes for the n = 3 States of Helium. III. Total Loss Rates for Normal Atom Collision. The Journal of Chemical Physics, vol. 56, Feb. 1972, pp. 1411-1412.

31. Rapp, D.; and Englander-Golden, P.: Total Cross Sections for Ionization and Attachment in Gases by Electron Impact. The Journal of Chemical Physics, vol. 43, Sept. 1965, pp. 1464-1479.

32. Dugan, J. L. G.; Richards, H. L.; and Muschlitz, E. G.: Excitation of the Metastable States of Helium by Electron Impact. The Journal of Chemical Physics, vol. 46, Jan. 1967, pp. 346-351.

33. Holt, H. F.; and Krotkov, R.: Excitation of n = 2 States in Helium by Electron Bombardment. Physical Review, vol. 144, April 1966, pp. 82-93.

34. Cermak, V.: Individual Efficiency Curves for the Excitation of 2^3S and 2^1S States of Helium by Electron Impact. Journal of Chemical Physics, vol. 44, May 1966, pp. 3774-3780.

35. Ferendeci, A. M.: Electron Excitation Cross Section of the He 2^1S State from Diffraction Losses in a He - Ne Gas Laser. Physical Review A, vol. 11, May 1975, pp. 1576-1582.

36. St. John, R. M.; Miller, F. L.; and Lin, C. C.: Absolute Excitation Cross-Sections of Helium. Physical Review, vol. 134, May 1964, pp. A888-A897.

37. Showalter, J. G.; and Kay, R. B.: Absolute Measurement of Total Electron-Impact Cross Sections to Singlet and Triplet Levels in Helium. Physical Review A, vol. 11, June 1975, pp. 1899-1910.

38. Jobe, J. D.; and St. John, R. M.: Absolute Measurements of the 2^1P and 2^3P Electron Excitation Cross-Sections of Helium Atoms. Physical Review A, vol. 164, Dec. 1967, pp. 117-121.

39. Kieffer, L. J.: Low-Energy Electron-Collision Cross-Section Data. Part II: Electron-Excitation Cross Section. Atomic Data, vol. 1, Nov. 1969, pp. 121-187.

40. Moiseiwitsch, B. W.; and Smith, S. J.: Electron Impact Excitation of Atoms. Reviews of Modern Physics, vol. 40, April 1968, pp. 124-353.

41. Phelps, A. V.: Absorption Studies of Helium Metastable Atoms and Molecules. Physical Review, vol. 99, Aug. 1955, pp. 1307-1313.

42. Benson, R. S.; and Kulander, J. L.: Electron Impact Excitation Rates for Helium. Solar Physics, vol. 27, Dec. 1972, pp. 305-318.

43. Wellenstein, H. F.; and Robertson, W. W.: Collisional Relaxation Processes for the n = 3 States of Helium. I. Excitation Transfer by Normal Atoms and by Electrons. The Journal of Chemical Physics, vol. 56, Feb. 1972, pp. 1072-1076.

44. Baker, D. J.; Bedo, D. E.; and Tomboulian, D. H.: Continuous Photoelastic Absorption Cross Section of Helium. Physical Review, vol. 124, Dec. 1971, pp. 1471-1476.

45. Lowry, J. F.; Tomboulian, D. H.; and Ederer, D. L.: Photoionization Cross Section of Helium in the 100- to 250- Å Region. Physical Review A, vol. 137, Feb. 1965, pp. 1054A-1057A.

46. St. John, R. M.; and Nee, T. W.: Collisional Transfer of Excitation Energy in Helium. Journal of the Optical Society of America, vol. 55, April 1965, pp. 426-432.

47. Jobe, J. D.; and St. John, R. M.: Excitation of the 4F States of Helium. Journal of the Optical Society of America, vol. 57, Dec. 1967, pp. 1449-1451.

48. Allison, D. C.; Browne, J. C.; and Dalgarno, A.: Collision Induced Deactivation of Metastable Helium. Proceedings of the Physical Society, vol. 89, Sept. 1966, pp. 41-44.

49. Collins, C. B.; Johnson, B. W.; and Shaw, M. J.: Study of Excitation Transfer in a Flowing Helium Afterglow Pumped with a Tuneable Dye Laser. I. Measurement of the Rate Coefficient for Selected Quenching Reactions Involving $He(5^3P)$. Journal of Chemical Physics, vol. 57, Dec. 1972, pp. 5310-5316.

50. Hurt, W. B.: Cross Section for the Reaction $He(2^3S) + He(2^3S)$. Journal of Chemical Physics, vol. 45, Oct. 1966, pp. 2713-2714.

51. Biondi, M. A.: Charged-Particle Recombination Processes. Defense Nuclear Agency Reaction Rate Handbook, Bartner, M. H. and Baurer, T., eds., Second ed., 1972, Chapter 16.

52. Warneck, P.: Studies of Ion-Neutral Reactions by a Photoionization Mass-Spectrometer Technique. IV. Reactions of He^+ with N_2 and O_2. Journal of Chemical Physics, vol. 47, Nov. 1967, pp. 4279-4281.

53. Schmeltekopf, A. L.; and Fehsenfeld, F. C.: De-excitation Rate Constants for Helium Metastable Atoms with Several Atoms and Molecules. Journal of Chemical Physics, vol. 53, Oct. 1970, pp. 3173-3177.

54. Mark, T. D.; and Oskam, H. J.: Ion Production and Loss Processes in Helium-Nitrogen Mixtures. Physical Review A, vol. 4, Oct. 1971, pp. 1445-1452.

55. Gabriel, H. A.; and Heddle, D. W. O.: Excitation Processes in Helium. Proceedings of the Royal Society of London, vol. 258, Nov. 1960, pp. 124-145.

56. Wiese, W. L.; Smith, M. W.; and Glennon, B. M.: Atomic Transition Probabilities. I. Hydrogen through Neon. NSRDS-NBS 4, National Bureau of Standards, Washington, D. C., 1966.

57. Cohen, J. S.: Diabatic-States Representation for $He^{*}(n \geq 3)$ + He Collisions. Physical Review A, vol. 13, Jan. 1976, pp. 86-98.

58. Bennett, W. R.: Optical Spectra Excited in High Pressure Noble Gases by Alpha Impact. Annals of Physics, vol. 18, June 1962, pp. 367-420.

59. Schneider, R. T.: On the Feasibility of Nuclear Pumping of Gas Lasers. Laser Interactions and Related Plasma Phenomenom, vol. 3, H. J. Schwartz and H. Hora, eds., Plenum Publishing Co., New York, 1974, pp. 85-107.

60. Hirschfelder, J. O.; Curtis, C. F.; and Bird, R. B.: Molecular Theory of Gases and Liquids. Second ed., John Wiley and Sons, New York, 1964, pp. 1110-1111.

61. Good, R. J.; and Hope, C. J.: New Combining Rule for Intermolecular Distance in Intermolecular Potential Functions. The Journal of Chemical Physics, vol. 53, July 1970, pp. 540-543.

62. Good, R. J.; and Hope, C. J.: Test of Combining Rules for Intermolecular Distances. Potential Function Constants from Second Virial Coefficients. The Journal of Chemical Physics, vol. 55, July 1971, pp. 111-116.

63. Neufeld, P. D.; Janzen, A. R.; and Aziz, R. A.: Empirical Equations to Calculate 16 of the Transport Collision Integrals $\Omega^{(\ell,S)*}$ for the Lennard-Jones (12-6) Potential. The Journal of Chemical Physics, vol. 57, Aug. 1972, pp. 1100-1102.

64. Kieffer, L. J.: A Compilation of Electron Collision Cross Section Data for Modeling Gas Discharge Lasers. JILA Information Center Report 13, Sept. 1973, Information Center, Joint Institute for Laboratory Astrophysics, University of Colorado, Boulder, Colorado.

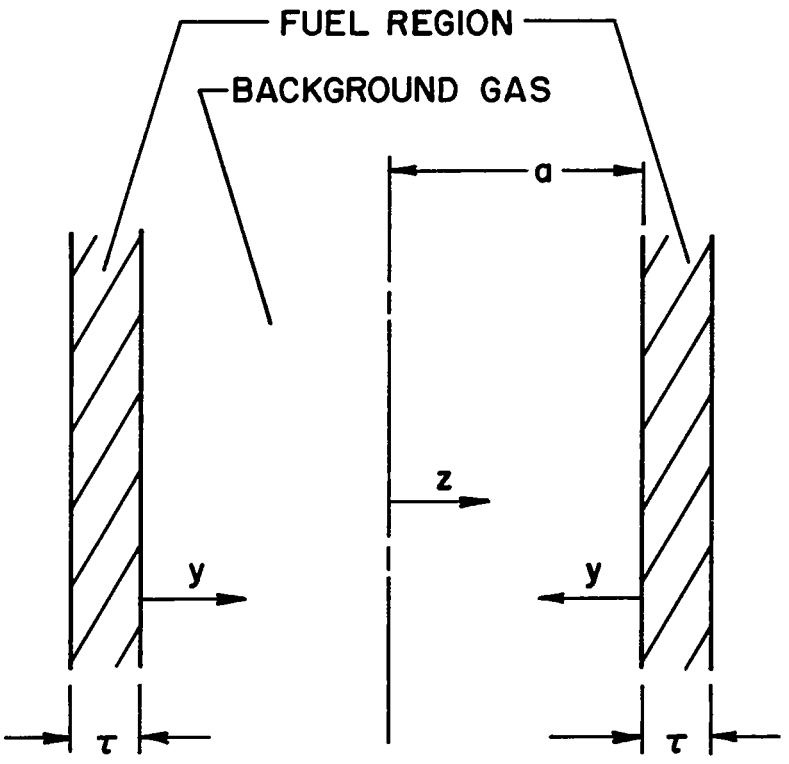

Figure 1. Slab approximation of cylindrical geometry.

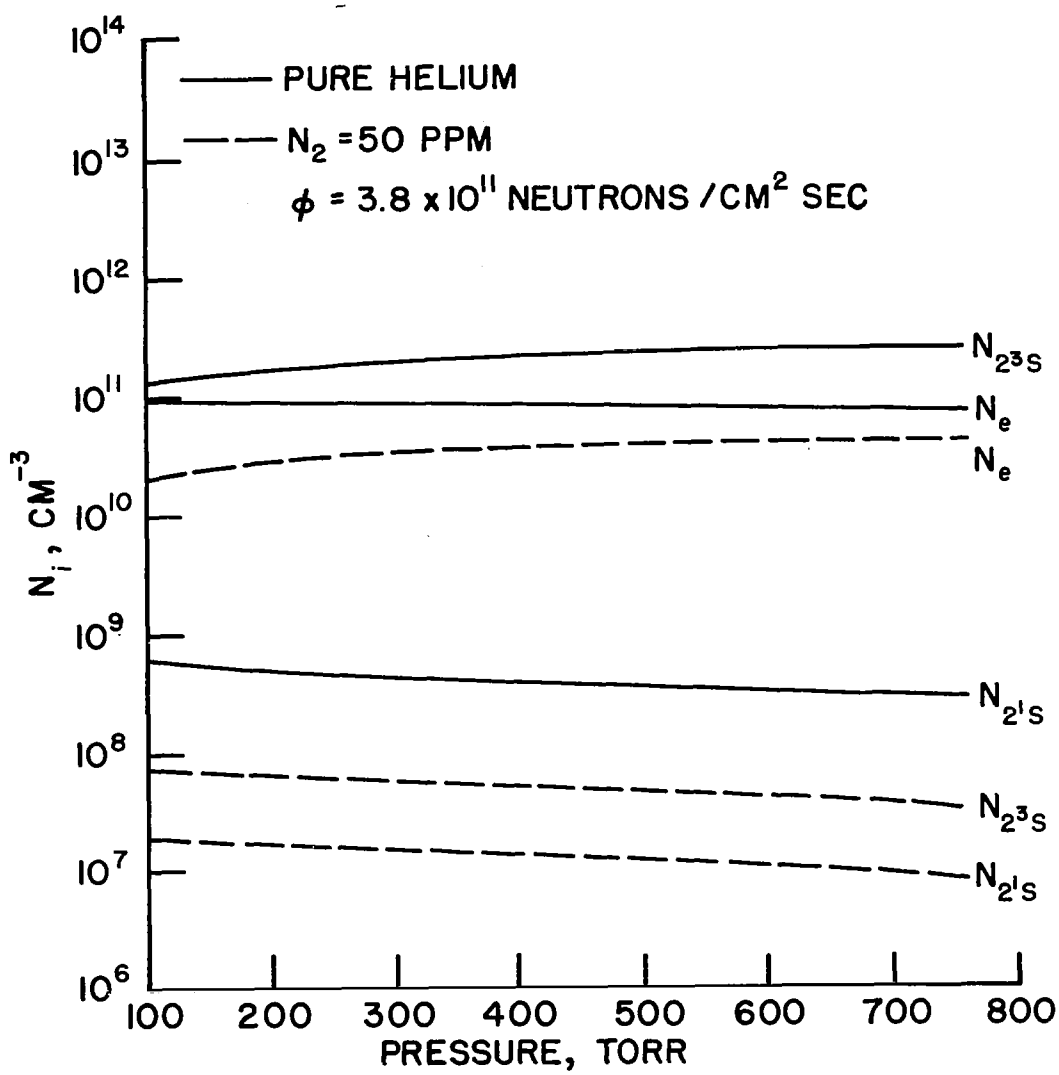

Figure 2. Influence of pressure on electron and metastable number densities.

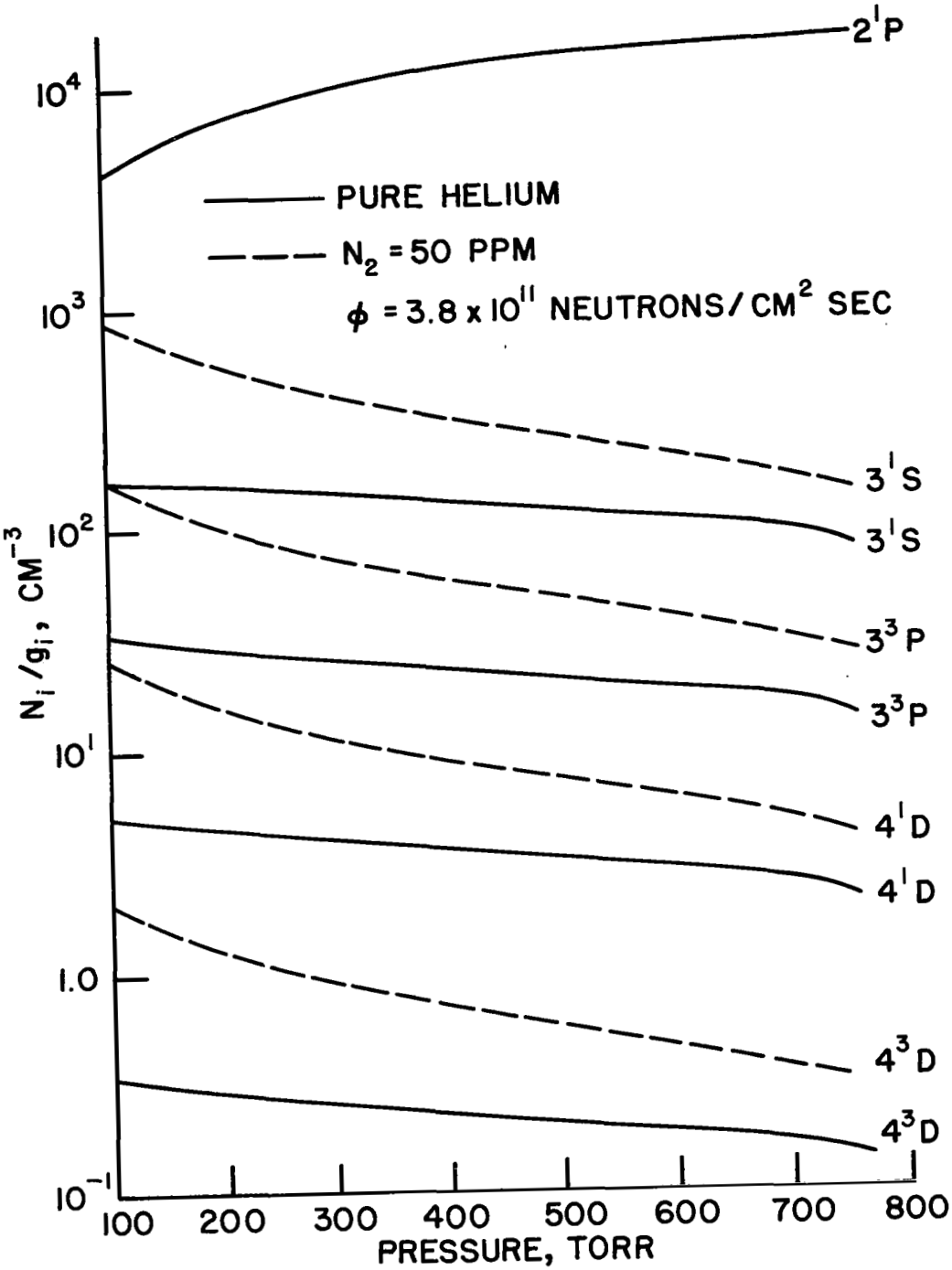

Figure 3. Influence of pressure on selected excited state number densities.

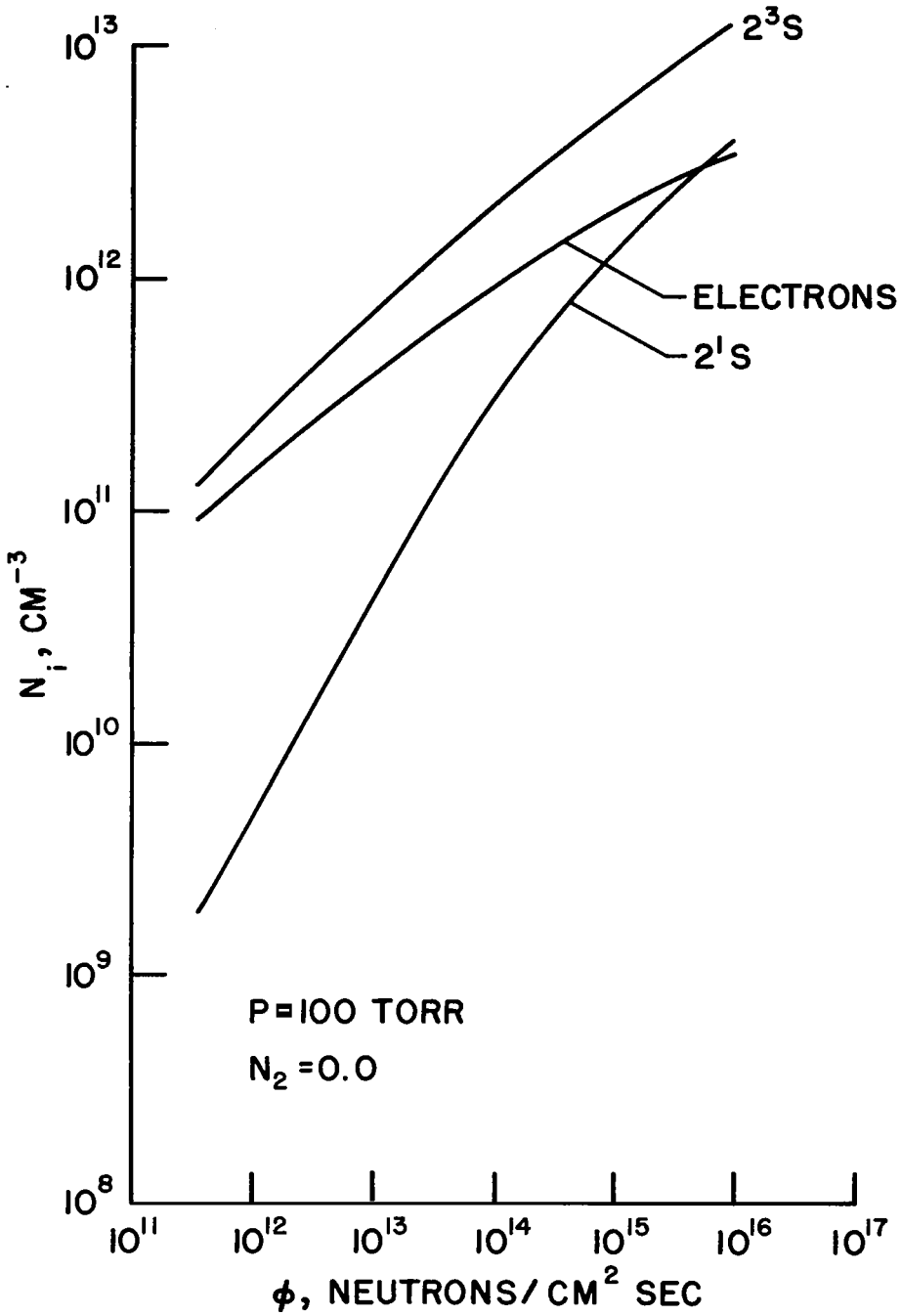

Figure 4. Effect of neutron flux on electron and metastable number densities.

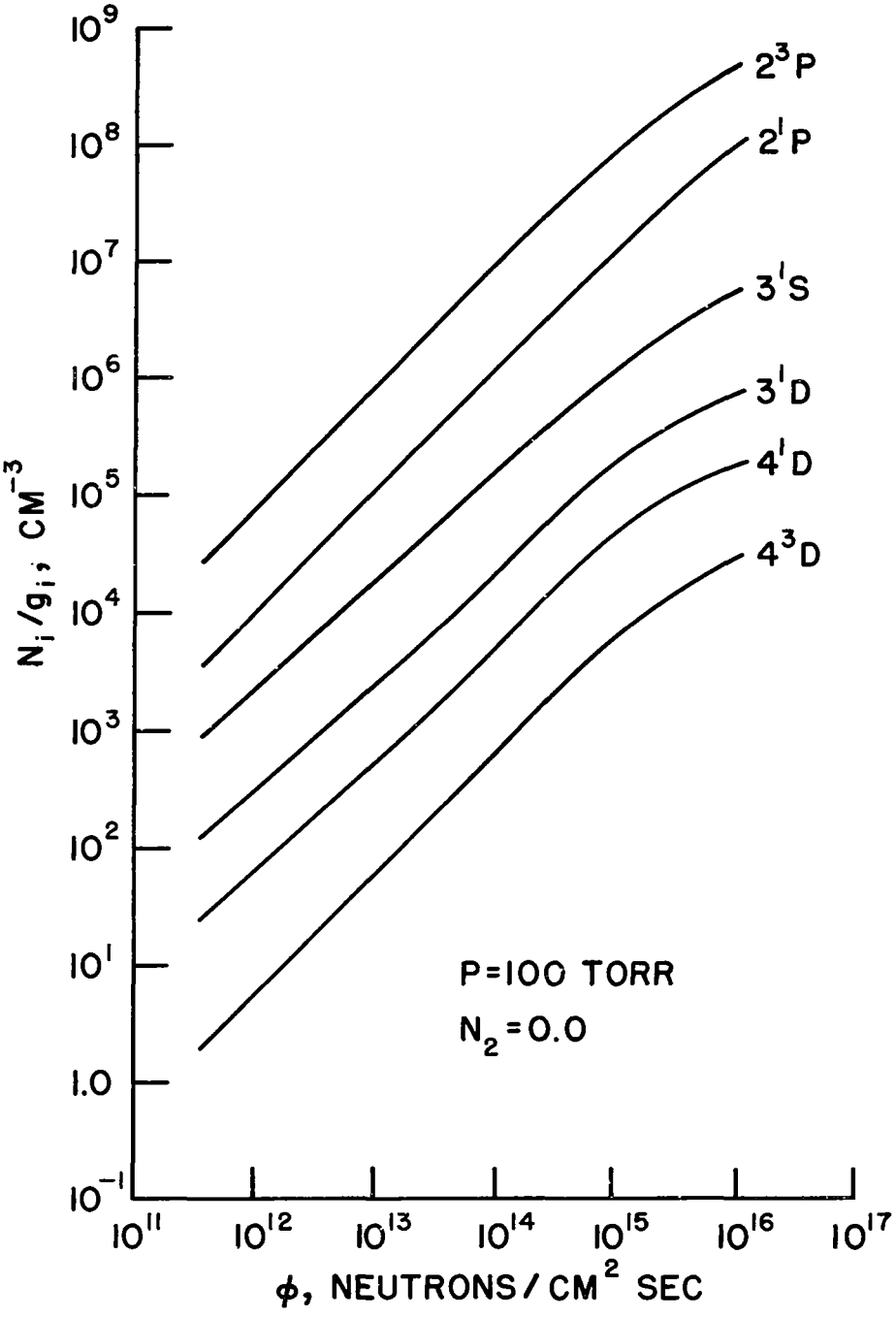

Figure 5. Effect of neutron flux on the number densities of some excited states.

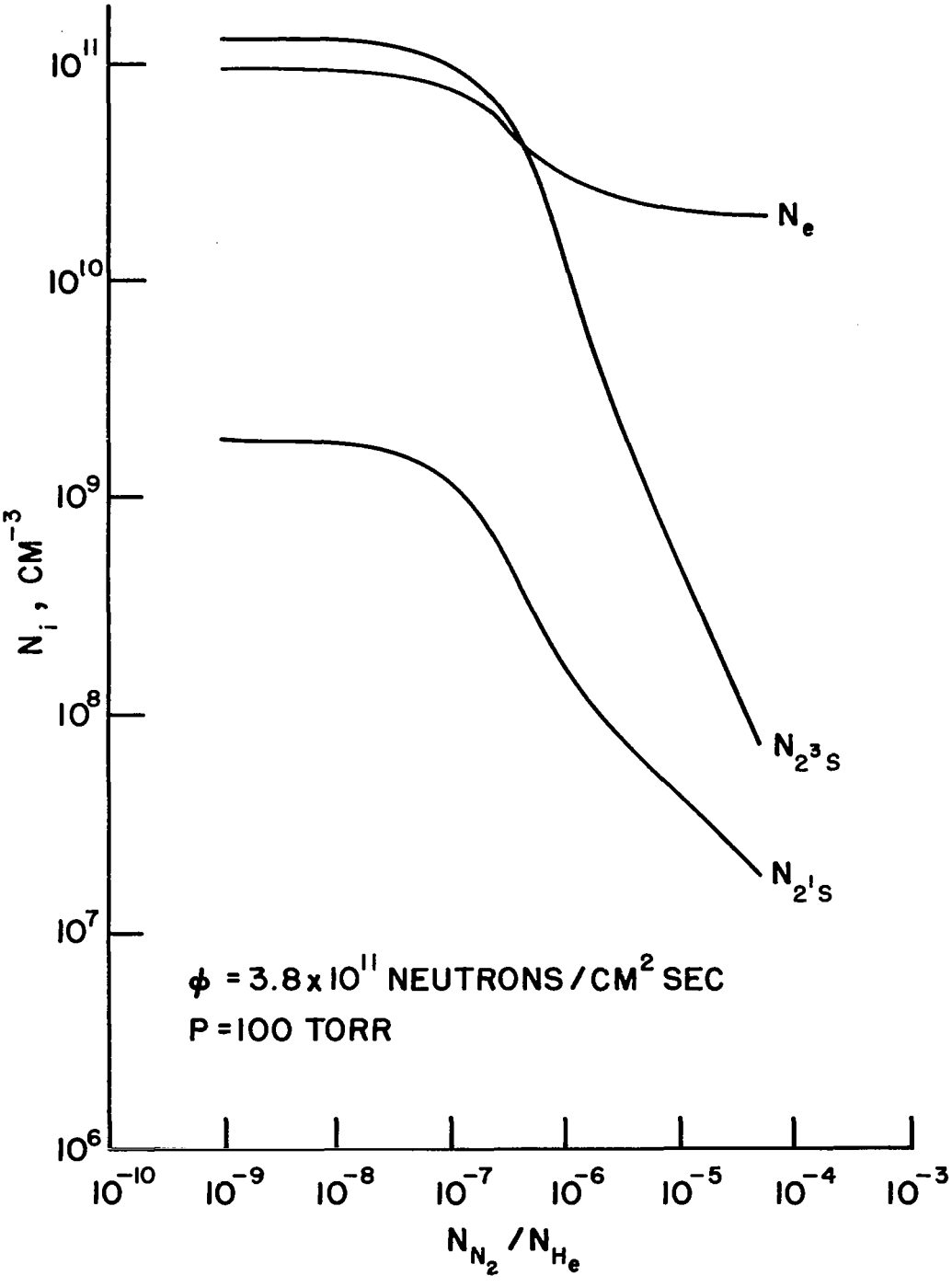

Figure 6. Effect of a nitrogen contaminant on electrons and metastables.

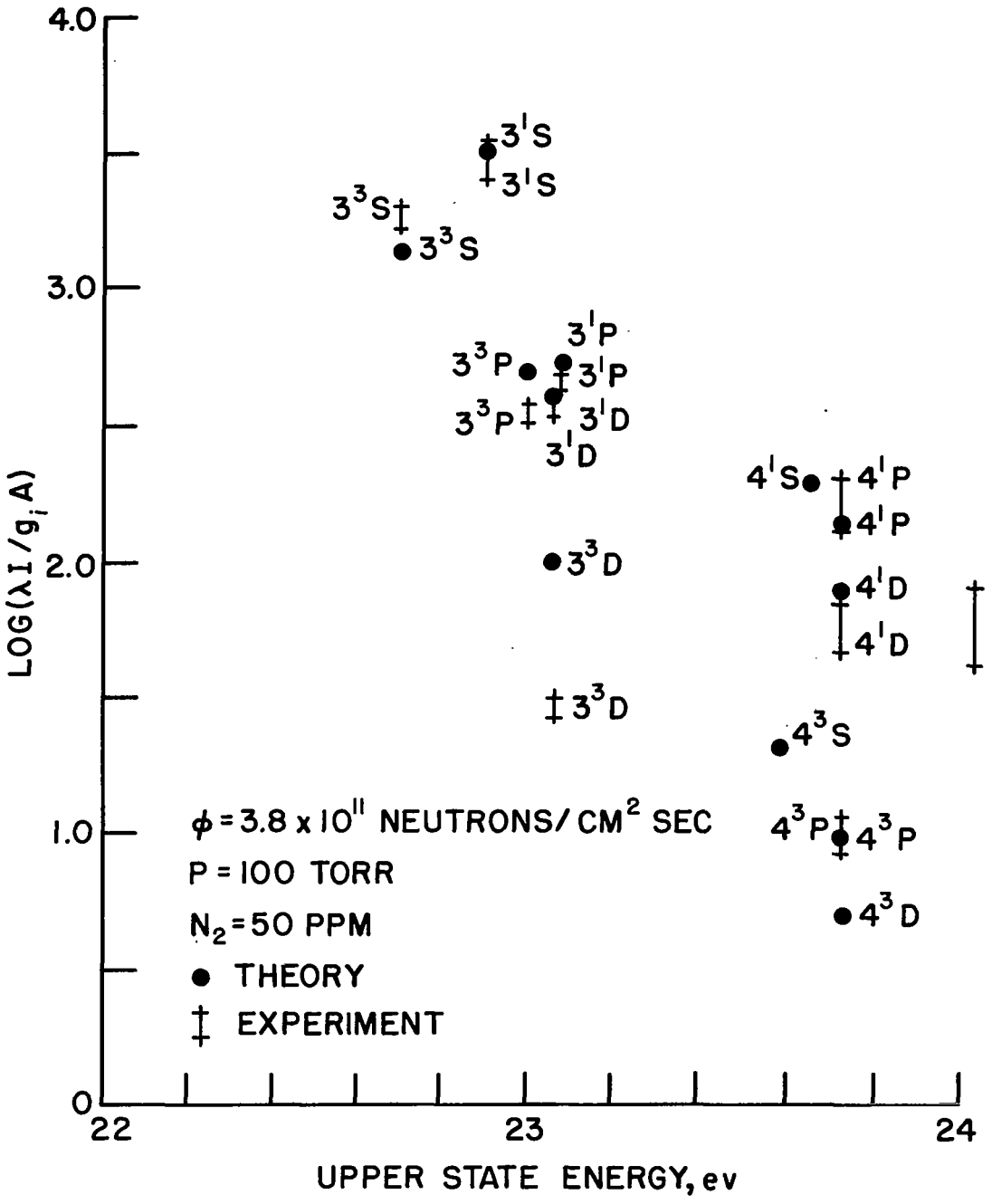

Figure 7. Helium excited states at 100 Torr, 2^1P model.

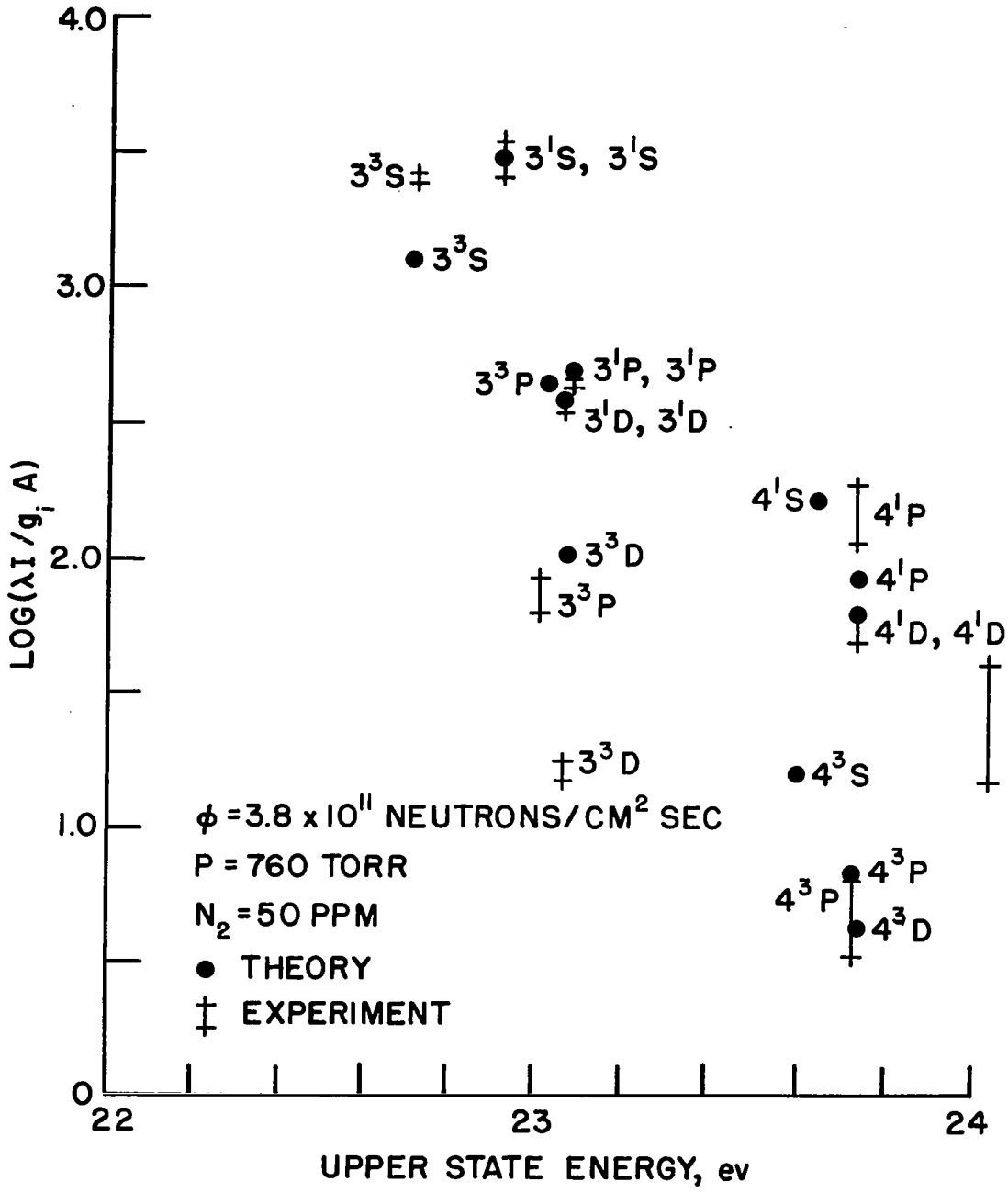

Figure 8. Helium excited states at 760 Torr, 2^1P model.

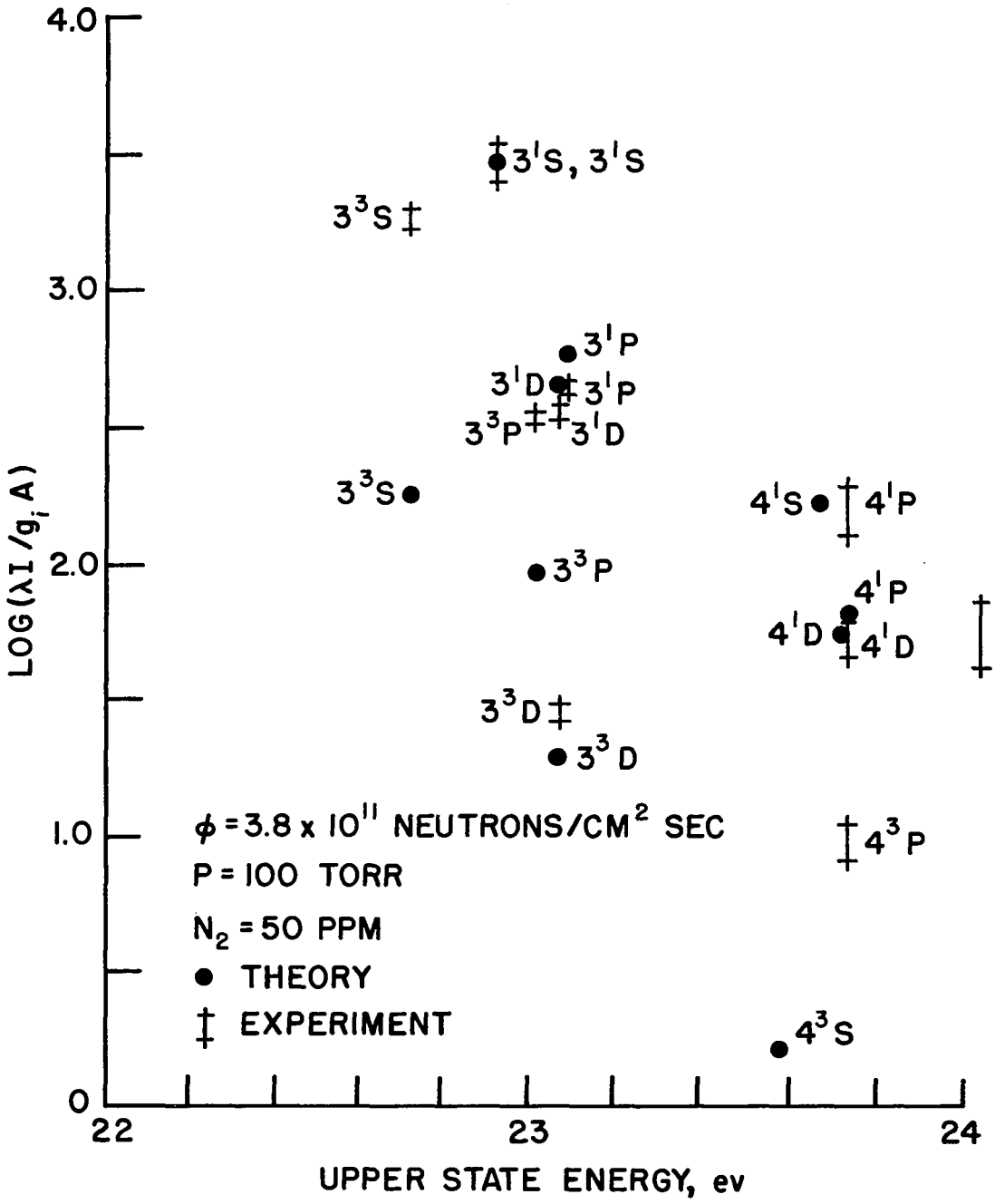

Figure 9. Helium excited states at 100 Torr, TM model.

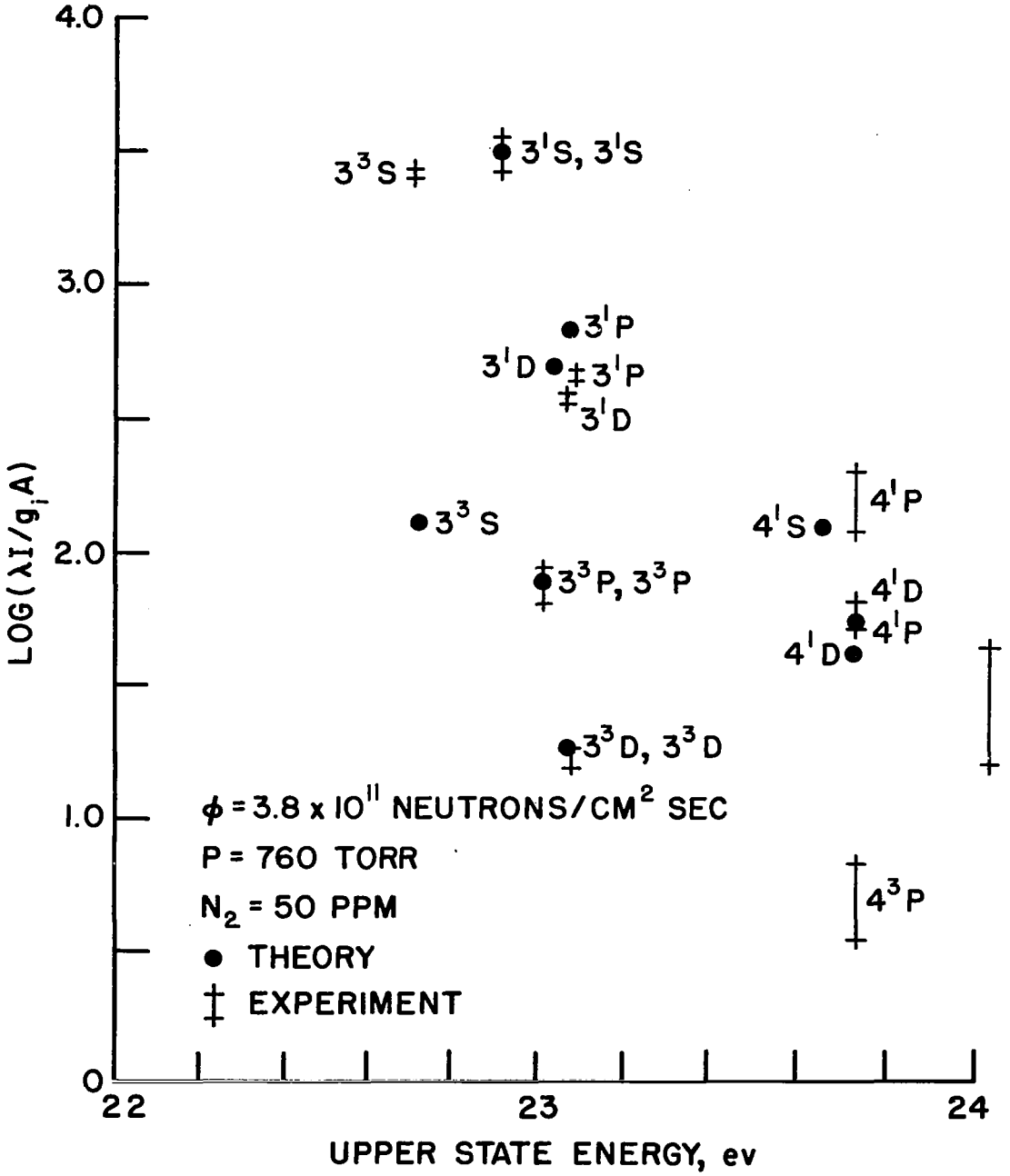

Figure 10. Helium excited states at 760 Torr, TM model.

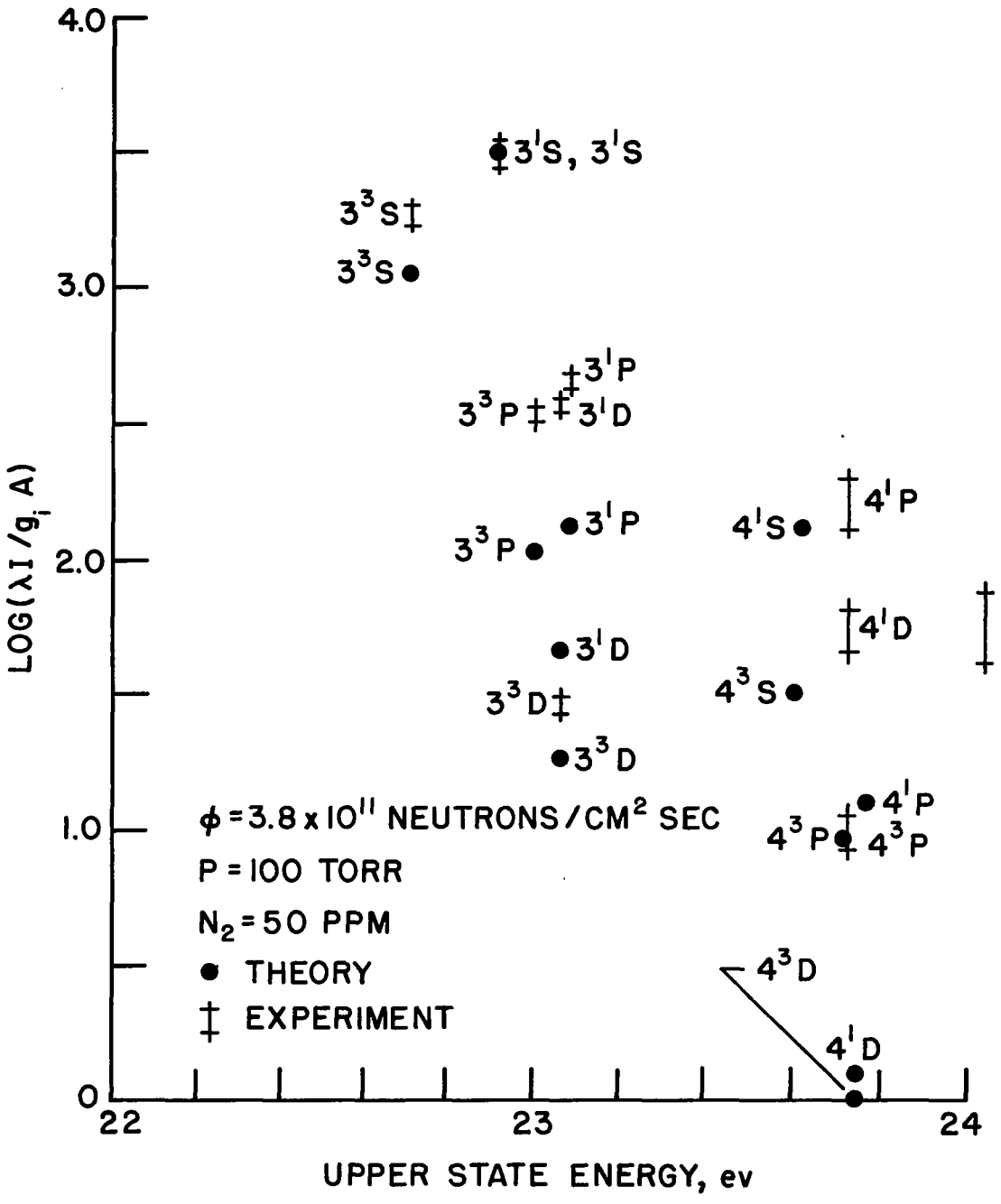

Figure 11. Effect of excitation transfer reactions on excited states.

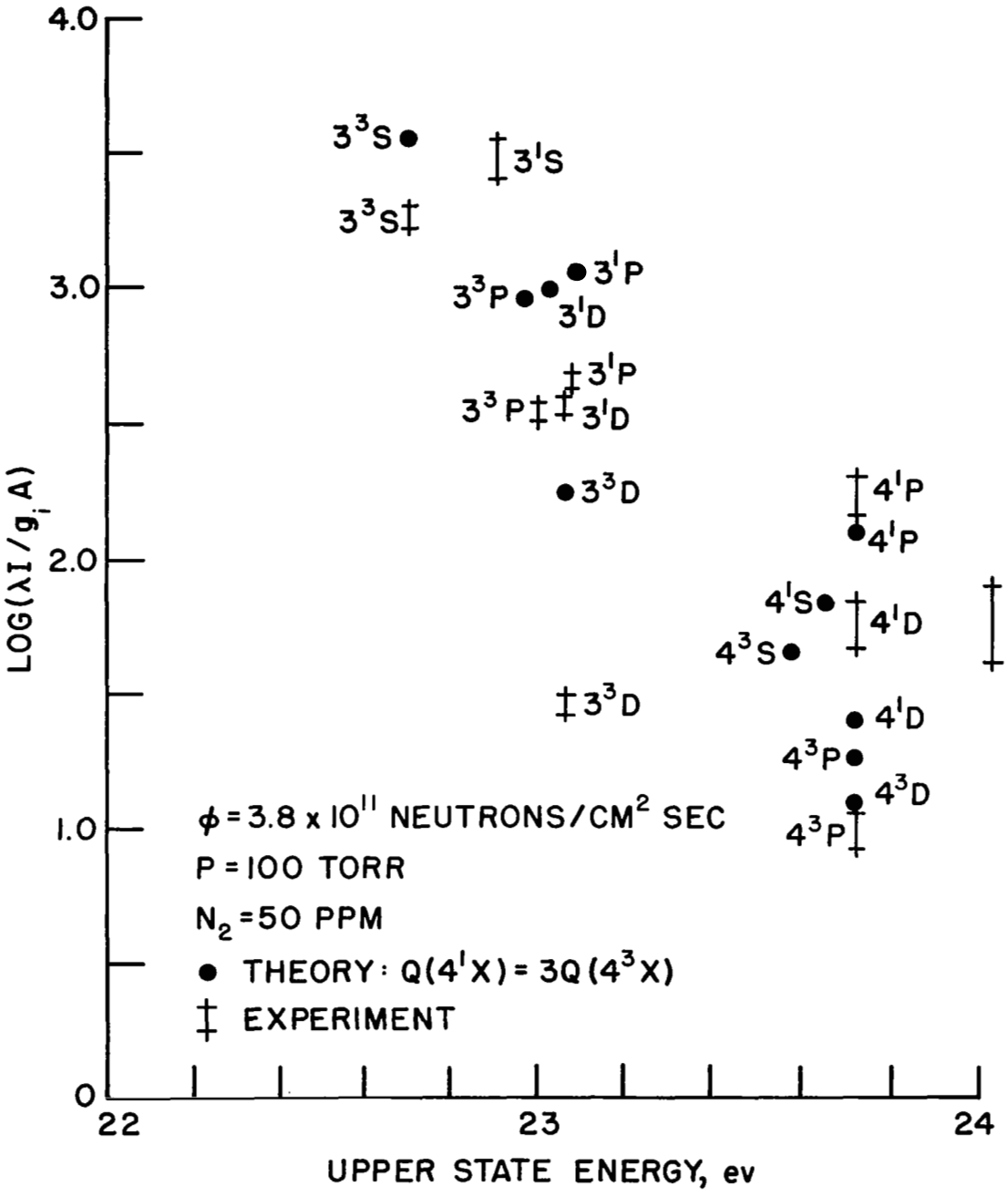

Figure 12. Effect of associative ionization and excitation transfer rates for n = 4 on excited states.

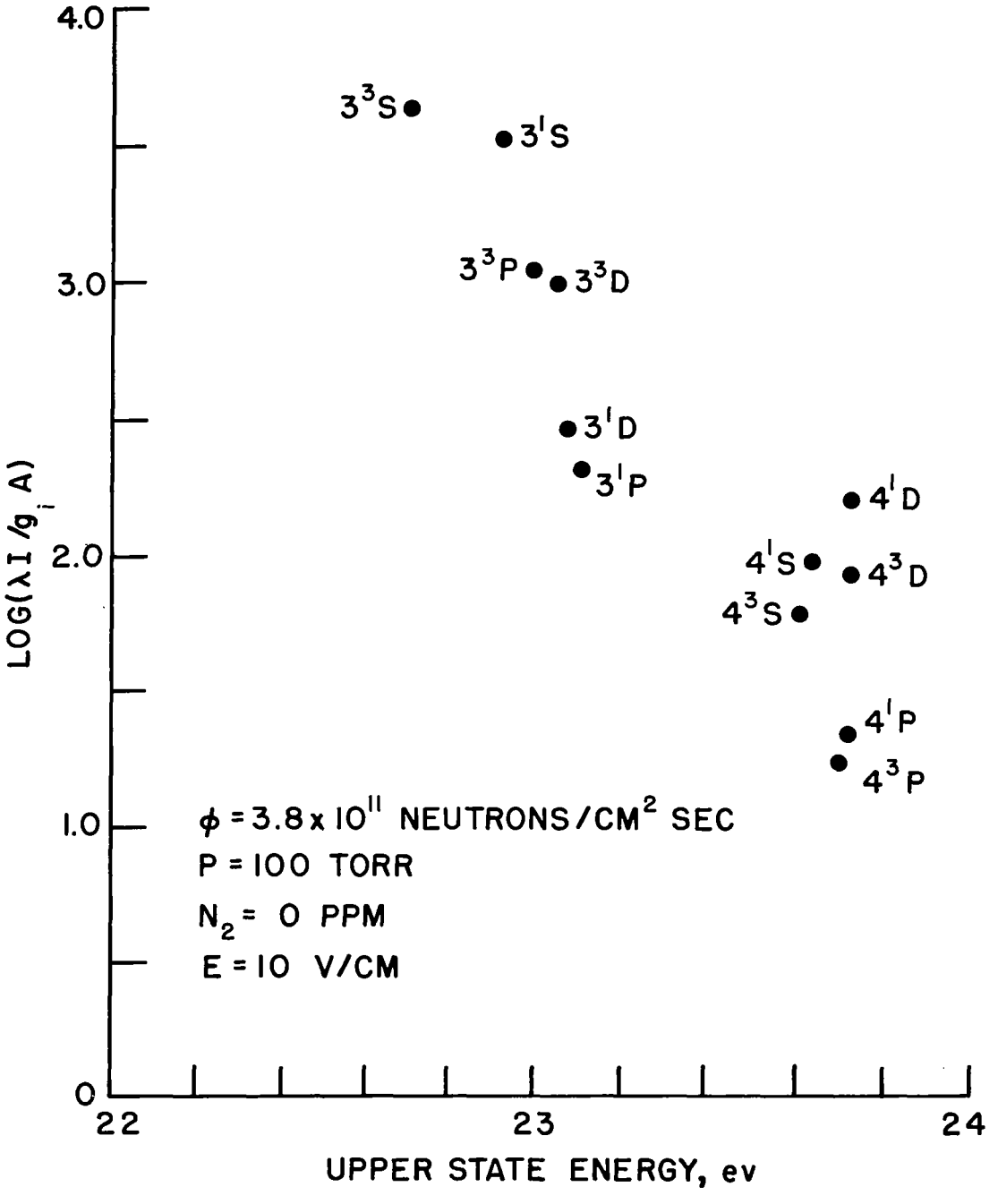

Figure 13. Influence of an externally applied electric field on excited states.